npj | flexible electronics

www.nature.com/npjflexelectron

ARTICLE OPEN

Check for updates

Flexible unimodal strain sensors for human motion detection and differentiation

Lu Jin[1,2], Zhenhong Li[3], Zekun Liu[1], Bethany Richardson[1], Yan Zheng[1], Lulu Xu[1], Zhongda Chen[1], Heng Zhai[1], Hongdoo Kim[4], Qingwen Song[2]✉, Pengfei Yue[2], Sheng Quan Xie[3,5]✉, Kap Jin Kim[4]✉ and Yi Li[1,2]✉

Multiple strain sensors are required to identify individual forces/stresses on human joints and recognize how they work together in order to determine the motion's direction and trajectory. However, current sensors cannot detect and differentiate the individual forces/stresses and their contributions to the motion from the sensors' electrical signals. To address this critical issue, we propose a concept of unimodal tension, bend, shear, and twist strain sensors with piezoelectric poly L-lactic acid films. We then construct an integrated unimodal sensor (i-US) using the unimodal sensors and prove that the i-US can detect and differentiate individual strain modes, such as tensioning, bending, shearing, and twisting in complex motion. To demonstrate the potential impact of unimodal sensors, we design a sleeve and a glove with the i-US that can capture wrist motions and finger movements. Therefore, we expect unimodal strain sensors to provide a turning point in developing motion recognition and control systems.

npj Flexible Electronics (2022)6:74 ; https://doi.org/10.1038/s41528-022-00205-4

INTRODUCTION

Human motion detection and differentiation are important for soft human-machine interaction[1,2], entertainment[3,4], and rehabilitation[5,6]. Several techniques have been developed to measure human motions. One approach utilizes the camera-based motion capture system to record a subject's detailed movements, but it requires high computational loads and can only be used to detect activities in a limited space[7,8]. Another method is to apply inertial sensors, but the sensors' rigidity confines their application in daily life[9,10]. More importantly, both systems cannot measure the individual forces/stresses of the motion. Alternatively, flexible and lightweight strain sensors, such as piezoelectric sensors, resistive sensors, capacitive sensors, triboelectric sensors, and so forth, provide a promising way for motion monitoring[11–18]. However, the vast majority of human body joints have multiple degrees of freedom[19–21], which involves multimodal forces/stresses such as tension, bend, shear, and twist that jointly determine the motion direction and trajectory. To measure the complicated individual joint motion precisely, multiple sensors are required to detect and differentiate the individual forces/stresses and identify their contributions at the desired positions. Some sensor networks have been developed for this purpose, which restrict the naturalness of movements[22–27] due to their size and the number of sensors required. In addition to such inefficiency and impracticality, these sensors cannot detect and differentiate the individual forces/stresses and their contributions to the motion from the sensors' electrical signals. For instance, the wrist has multiple degrees of freedom; it can bend, twist, and even rotate[22,28]. Electrical signals can detect from the sensors attached to the wrist joint once deformed. However, the electrical signals can not identify what forces are involved and how they work together to determine the motion because these sensors do not have such capabilities. Therefore, it is essential to develop a type of strain sensor that can detect and differentiate individual forces/stresses by eliminating their coupling effects, which can be further integrated to identify the contribution of specific individual forces/stresses in a complex motion to enable the recognition of motion patterns from the signals of individual sensor. This function is extremely important for motion monitoring and control, as the motion trajectory and movement are determined by the joint force of individual stresses.

Hence, we propose a concept of unimodal strain sensors with uniaxially drawn piezoelectric poly L-lactic acid (PLLA) films and then combine them into an integrated unimodal sensor (i-US), which can detect and differentiate typical deformations, such as tensioning, bending, shearing, and twisting with eliminating the coupling effects from compression.

RESULTS AND DISCUSSION

Theoretical background of unimodal strain sensors

We first design four unimodal tension, bend, shear, and twist strain sensors with piezoelectric PLLA films, which only respond to tensioning, bending, shearing, and twisting. The pristine piezoelectric PLLA film only presents a shear piezoelectric coefficient (PC), i.e., d_{14}, because of its helical structure[29]. It is usually cut at a certain angle from the crystal orientation (i.e., drawing direction) of the original PLLA sheet to respond to an external stimulus via modifying its PC[30]. We, therefore, calculated PCs of four PLLA films with particular cutting angles (CA) such as 45°, −45°, 0°, and 90° through a mathematical model of the PCs of PLLA film. Of particular interest is that two normal PCs, along with the width and length directions (d_{12}' and d_{13}'), are newly created in the PLLA films with CAs of 45° and −45°, named PLLA45 and PLLA-45; simultaneously, the primary shear PC, d_{14}, disappears. Besides, the two normal PCs of PLLA45 are opposite to those of PLLA-45. In contrast, the PLLA films with CAs of 0° and 90°, called PLLA0 and PLLA90, only have the shear PC; they are opposite each other (see

[1]Department of Materials, School of Natural Sciences, The University of Manchester, Manchester, UK. [2]College of Textile Science and Engineering, Xi'an Polytechnic University, Xi'an, China. [3]School of Electronic and Electrical Engineering, University of Leeds, Leeds, UK. [4]Department of Advanced Materials Engineering for Information and Electronics, Kyung Hee University, Yongin, South Korea. [5]Institute of Rehabilitation Engineering, Binzhou Medical University, Yantai, China. ✉email: 1143601883@qq.com; S.Q.Xie@leeds.ac.uk; kjkim@khu.ac.kr; henry.yili@manchester.ac.uk

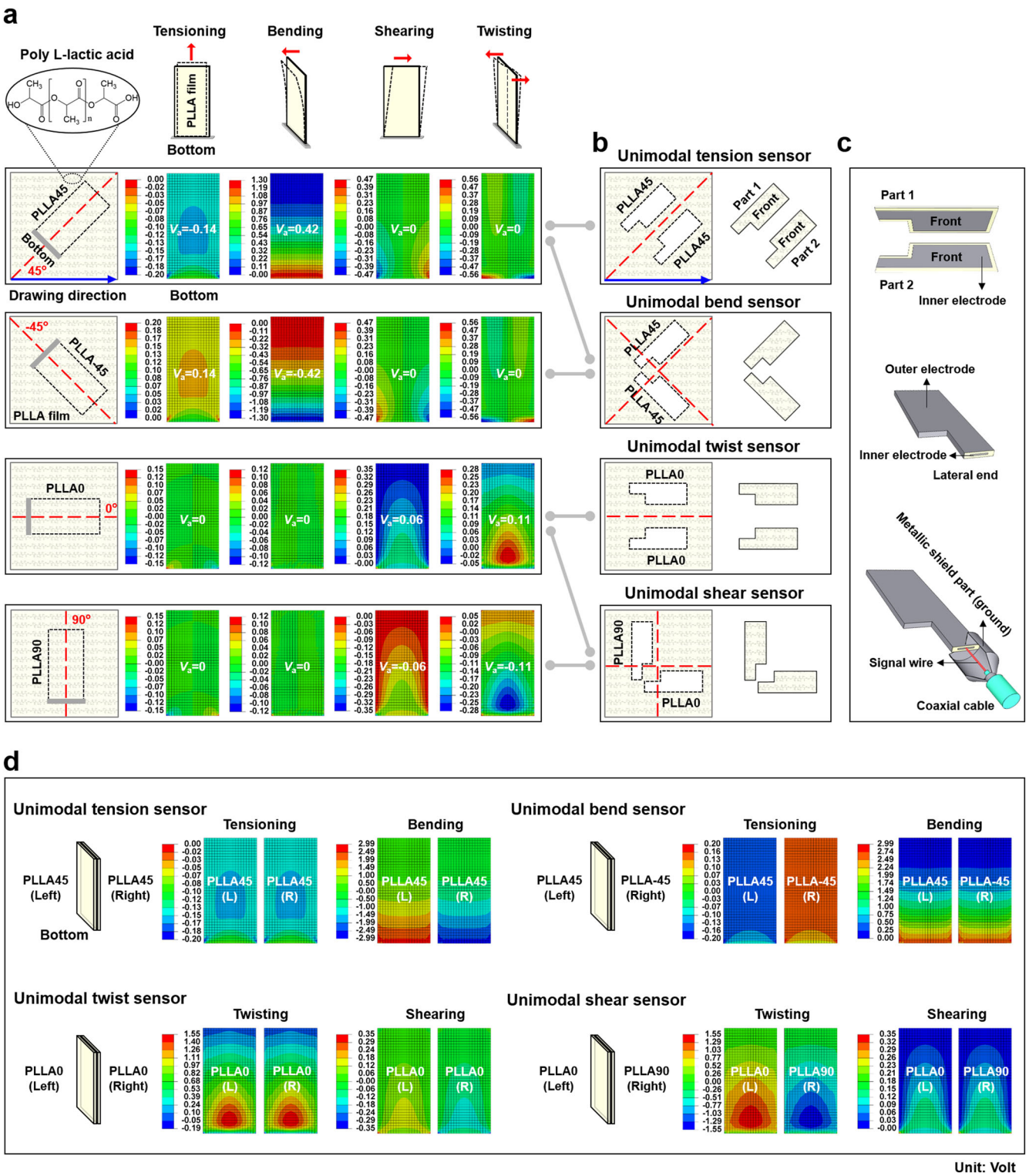

Supplementary Note 1). We then analyzed the piezoelectric responses of the four PLLA films when subjected to typical deformations, such as tensioning, bending, shearing, and twisting via finite element simulations using ABAQUS. To confirm the independence of simulation results from discretization resolution, we first examined the effect of the resolution on the results through a mesh refinement procedure (Supplementary Fig. 2). The deformation directions of tensioning, bending, and shearing in simulations cover three axes of a 3-D cartesian system, as shown in the top schematic of Fig. 1a. Notably, a more complex twisting deformation is considered in this work. Thus, these four basic deformation components will introduce any morphologic change to the PLLA film. The PLLA45 and PLLA-45 are sensitive to tensioning and bending deformations because the average voltage of all nodes of each PLLA film surface (V_a) is non-zero. Moreover, the generated voltages of each sample are vertically

Fig. 1 Design concept of unimodal tension, bend, twist, and shear sensors. a Top schematics show the applied forces and their directions for tensioning, bending, shearing, and twisting deformations in finite element simulations. The bottom panels show the piezoelectric response simulations of the uniaxially drawn piezoelectric PLLA films with different cutting angles under tensioning, bending, shearing, and twisting deformations. The first panel shows the piezoelectric PLLA film with a cutting angle of 45° (PLLA45) and its cutting schematic (first graph) with a cutting shape (black dash line) and a cutting angle (red dash line). The average responding voltage of all nodes of the PLLA film surface (V_a) is shown in the middle. The same illustrative schemes are applied for PLLA-45, PLLA0, and PLLA90. **b** Left schematics show the cutting angles and cutting shapes of two PLLA parts from an original PLLA film for the unimodal sensors, and the right schematics show the corresponding parts after cutting out; **c** Top schematic shows the patterns of inner electrodes, and the front sides of two parts of each sensor are stuck together; the middle one shows the exposed area of each assembled sensor is coated with silver conductive paint as an outer electrode, except the lateral end of the sensor; the bottom one shows the inner electrodes are connected to a signal wire, and the outer electrode is connected to a metallic shield part (ground) of a coaxial cable. **d** Piezoelectric response simulations of two PLLA films composing each unimodal sensor under tensioning, bending, shearing, and twisting deformations to prove the unimodal sensors' hypothesis. The first panel shows the piezoelectric response of two PLLA45s of the unimodal tension sensor under tensioning and bending. The generated voltages of the two PLLA45s are superimposed when tensioned, but they are offset under bending. The unimodal tension sensor under twisting and shearing is not simulated because the PLLA45 is insensitive to the two deformations, as demonstrated in Fig. 1a. The same illustrative schemes are applied for the unimodal bend, twist, and shear sensors.

symmetrical, but they are opposite under shearing or twisting and thus offset each other inside (i.e., $V_a = 0$), not showing a piezoelectric response on the whole. This is attributed to the normal PCs of the PLLA45 and PLLA-45. Similarly, the PLLA0 and PLLA90 are only responsive to the shearing and twisting deformations because of the shear PCs (Fig. 1a and Supplementary Video 1). Overall, each PLLA film is still sensitive to two deformation modes, indicating that it is impossible to determine the exact deformation status with the piezoelectric signal measured from the single-layer PLLA film sensor during deformation. Crucially, we found that the PLLA45 and PLLA-45 generate opposite voltages under the same deformation, and so do PLLA0 and PLLA90.

Design concept and hypothesis of unimodal sensors

Based on the above findings, we introduce a double-layered PLLA film design concept of unimodal tension, bend, twist, and shear sensors, as illustrated in Fig. 1b, c. We hypothesize that as the unimodal tension sensor consists of two PLLA45s, both receive tensile stress when tensioned, producing the same charges in the inner and outer electrodes, respectively; the electric signals of two PLLA45s will be superimposed. Under bending, the upper area of each PLLA45 receives compressive stress, whereas the bottom area is relatively subjected to tensile stress, generating the opposite charges; the signals of two PLLA45s will be canceled out. The charges produced will also be offset inside each PLLA45 under twisting and shearing deformations, not showing a signal, as illustrated in Supplementary Fig. 3. Conversely, as the unimodal bend sensor is composed of PLLA45 and PLLA-45, the bend sensor's signal will be boosted under bending, but it will be offset when tensioned. To prove the design concept theoretically, the piezoelectric responses of both PLLA films of the unimodal tension, bend, twist, and shear sensors were simulated under different deformations. As long as the unimodal sensors receive their matched deformations, two PLLA films composing each unimodal sensor produce the same piezoelectricity; otherwise, they generate opposite voltages (Fig. 1d), which exactly agrees with our hypothesis.

Unimodal sensor fabrication

The piezoelectric property of uniaxially drawn PLLA film depends on its crystal orientation and crystallinity, which are dominated by fabrication conditions, especially the drawing ratio (DR)[29,31,32]. We, therefore, prepared four uniaxially drawn piezoelectric PLLA films with different DRs, such as 3.3, 3.7, 4.0, and 4.5 (Fig. 2a). As shown in Fig. 2b, the crystal orientation improves with increasing the DR because a Debye-Scherrer ring displayed at an initial DR of 3.3 gradually becomes three ellipses at a maximum DR of 4.5, indicating the highly orientated α-crystal structure is formed[33]. This behavior is observed by their melting thermograms as well. After a glass transition temperature (64 °C), the cold crystallization temperature of the drawn PLLA films appears at different temperatures, and the lower DR, the higher the crystallization temperature. This is because the low chain orientation of the PLLA film requires more energy to form the ordered arrangements and undergoes crystallization at a higher temperature (Fig. 2c). Besides, there is a single melting peak at around 170 °C, a typical α-crystal melting peak[29], but the β-crystal melting peak at 155 °C is not observed[34], further confirming all PLLA films are only composed of α-crystal. The crystallinity increases with increasing the DR, and it reaches 60.9% at a DR of 4.5 (Fig. 2d), because the stretching with more significant DR enhances the orientation degree of the crystal domains, promoting crystallization[31,33]. Due to the highest α-crystal orientation and crystallinity among all samples, the piezoelectric PLLA film with the DR of 4.5 exhibits the most superior piezoelectric response under the same tensioning, bending, twisting, and shearing conditions (Fig. 2e) and Supplementary Fig. 4 shows the SEM images of the PLLA film. We confirmed the polarity of the PLLA film with the DR of 4.5 by swapping the connection of the electrodes[35]. The PLLA film generates opposite piezoelectricity under the same tension force, indicating the output electric signal comes from the piezoelectricity (Supplementary Fig. 5). We also tested both transverse and longitudinal responses of the as-prepared PLLA film, proving that the PLLA film has only a shear PC (Supplementary Fig. 6). Therefore, the PLLA film with the DR of 4.5 was selected and fabricated into four unimodal tension, bend, twist, and shear sensors following the proposed design concept (Fig. 2f), and Fig. 2g shows the stress-strain curve of a unimodal tension sensor. Notably, as the prepared PLLA film with α-crystal (i.e., 10_3 helical structure) does not present a remnant polarization prior to any deformation, one cannot determine its resultant polarization direction without a measurement; in other words, which side of the PLLA film produces positive charges or negative charges when deformed. One, however, can hypothesize that the front sides of two PLLA45s certainly generate the same charge, and so do two PLLA0s; whereas those of the PLLA45 and PLLA-45 and the PLLA0 and PLLA90 undoubtedly produce the opposite charges in the identical deformation because they are cut from the same PLLA film sheet. Therefore, to facilitate the process of sensor fabrication, the front sides of the two matched PLLA parts are stuck to each other.

These unimodal sensors were tested under tensioning, bending, twisting, and shearing conditions. Comparing four unimodal sensors under the same deformation condition (i.e., horizontal comparison of Fig. 3a), each sensor exhibits the most significant piezoelectric behavior when receiving a matched stimulus; otherwise, there is almost no response. The same tendency is also observed at different deformation levels (P-value < 0.001,

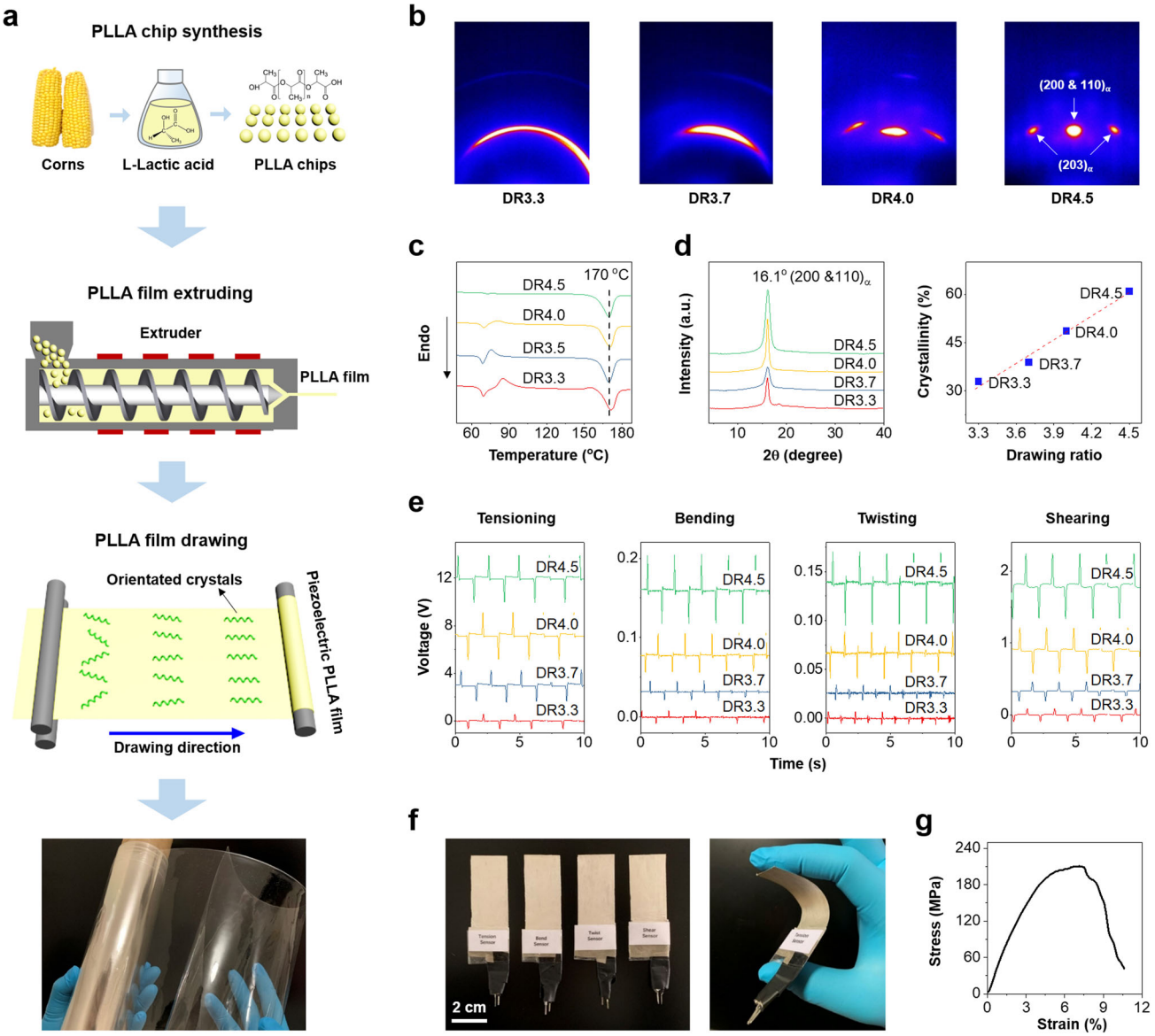

Fig. 2 Preparation and characterization of uniaxially drawn piezoelectric PLLA films. a Schematic of uniaxially drawn piezoelectric PLLA films preparation process. The first photograph shows the PLLA chip synthesis, which is polymerized from L-lactic acid that is obtained from the fermentation of renewable and biodegradable plant sources such as corns[41]. The second photograph shows the PLLA film extruding. The third photograph shows that PLLA film is stretched at different drawing ratios (DR) of 3.3, 3.7, 4.0, and 4.5 by two drawing rollers, and each sample named DR3.3, DR3.7, DR4.0, and DR4.5, respectively. The thickness of four PLLA samples is about 70 μm. The bottom photograph shows a transparent piezoelectric PLLA film (DR4.5). **b** Two-dimensional wide-angle x-ray diffraction (2D-WAXD) photographs of four PLLA film samples for crystal orientation analysis; (c) Differential scanning calorimeter (DSC) melting thermograms of the PLLA films with different DRs for crystal form determination. **d** 1D-WAXD spectrum of the PLLA films for crystal form determination (left) and their crystallinity (right). **e** Comparison of piezoelectric response of four PLLA film samples under tensioning (1% strain), bending (20° bent angle), twisting (30° twisted angle), and shearing (0.015 shear strain) deformation. The dimension (Length × Width) of each sensor is 4 × 2 cm. Each PLLA film is cut at 45° from the drawing direction for the tensioning and bending test and is cut at 0° for the shearing and twisting test. **f** Photographs of four unimodal sensors (left) and the sensor flexibility demonstration (right). **g** Stress-strain curve of a unimodal tension sensor.

Supplementary Fig. 7). Compared to unimodal sensors under matched deformations, a control made of unstretched PLLA film generates extremely low signals at all deformation levels, confirming that the electric signal of unimodal sensors originates from piezoelectricity. To further evaluate their piezoelectric behavior when subjected to different deformations, the corresponding peak to peak signal amplitudes ($V_{p\text{-}p}$) of Supplementary Fig. 7 are normalized (see Supplementary Methods) to compare all signals under the same scale. As expected, all unimodal sensors are sensitive to their corresponding deformations but insensitive to the other conditions (Fig. 3b). We also examined the stability and repeatability of the four unimodal sensors. The stable and continuous piezoelectric response during 10000 cycles and the reproduced piezoelectric signals after each day without significant variation demonstrate great signal stability and repeatability (Supplementary Fig. 8).

The unimodal tension sensor exhibits a relatively stronger piezoelectric noise signal than the other sensors under unmatched deformations (Fig. 3b). This is ascribed to the mismatching of two PLLA45s composing the tension sensor. The operating mechanism of these sensors is amplifying their signals when subjected to the corresponding stimuli but offsetting under

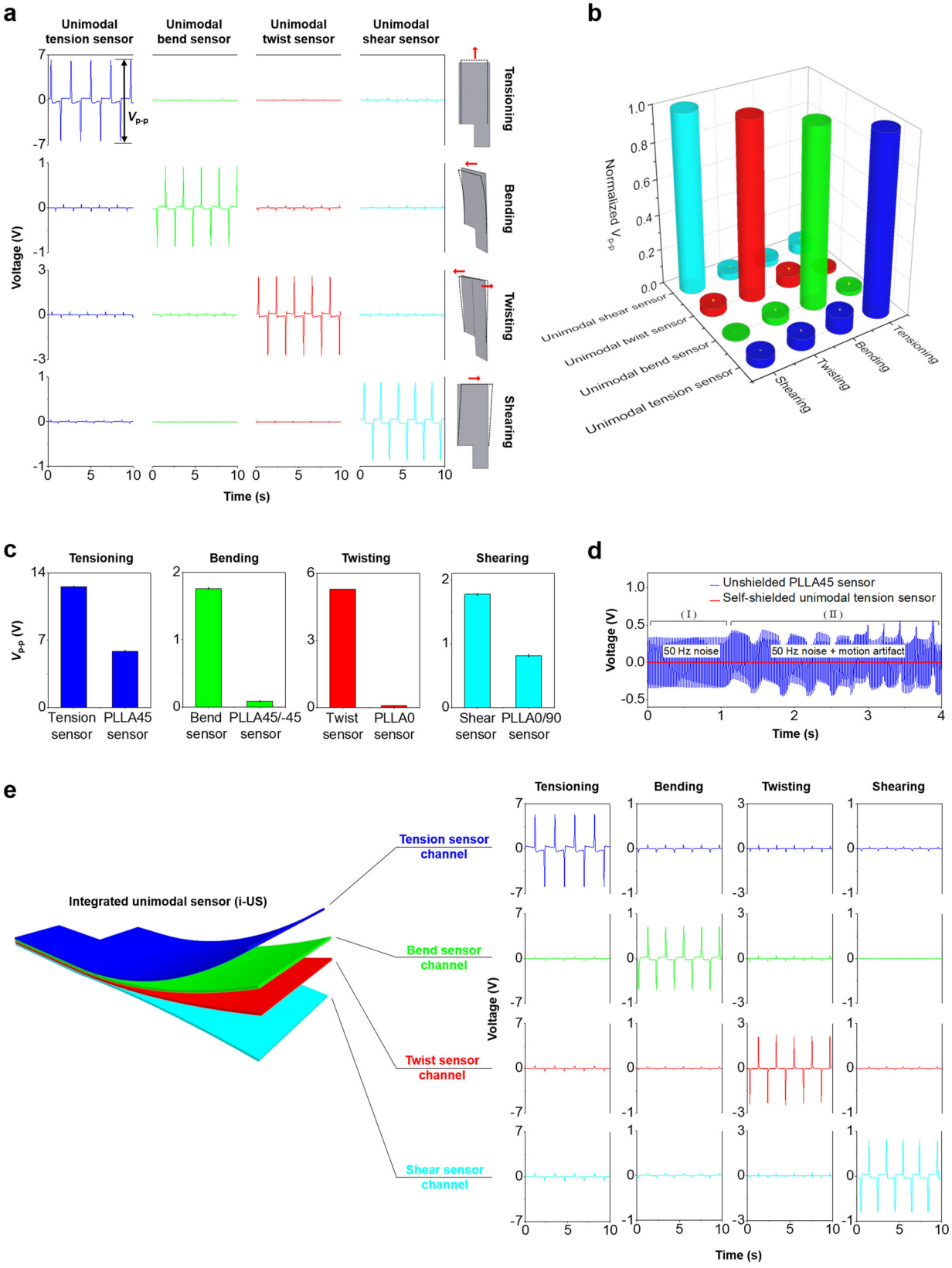

unmatched deformations. The latter is a key for unimodal sensors, and it is much more difficult to be achieved than the former. This is because a slight discordance in piezoelectric and physical properties of two PLLA films, such as CA, drawing direction, size, and thickness, could result in a non-negligible noise even under the non-corresponding stimuli. For instance, a slight deviation on the CA of the PLLA45 can cause the residual shear piezoelectric coefficient, d_{14}, in the PLLA45, which acts to shearing and twisting

Fig. 3 Performance evaluation of four unimodal sensors and integrated unimodal sensor (i-US). a Piezoelectric responses of each unimodal sensor under the same tensioning (1% strain), bending (20° bent angle), twisting (30° twisted angle), and shearing (0.015 shear strain) conditions. Schematics of unimodal tension, bend, twist, and shear sensors with their corresponding deformations are shown in right insets. **b** Normalized $V_{p\text{-}p}$ of unimodal tension, bend, twist, and shear sensors under tensioning, bending, twisting, and shearing deformation conditions. **c** Comparison of the piezoelectric response between the four unimodal sensors and the conventional single-layer PLLA sensors under the above conditions (Fig. 3a). **d** Shielding performance of the unshielded PLLA45 sensor and the self-shielded unimodal tension sensor (I) under the static condition and (II) when walking/running next to two sensors. **e** Schematic of the i-US comprising unimodal tension, bend, twist, and shear sensors (left). The right panels show the piezoelectric response of the i-US under the tensioning, bending, twisting, and shearing conditions. All conditions are the same as those used for individual unimodal sensor **a**.

deformations. The size or thickness difference can also lead to the uneven force received between two PLLA45s. To minimize such discrepancies, the two PLLA parts of each unimodal sensor should be cut from the same area of the original PLLA film, and the closer the two parts, the better the performance. Another difficulty in the unimodal sensor fabrication is finding the exact uniaxial drawing direction of the transparent PLLA film because an incorrect drawing direction could lead to an inevitable error in the CA.

We also evaluated the piezoelectric pressing responses of four unimodal sensors by comparing a commercial piezoelectric poly(vinylidene fluoride) (PVDF) film sensor. As shown in Supplementary Fig. 9, all unimodal sensors are insensitive to pressing, but the signal of the PVDF film sensor increases with increasing the applied pressure. Both PLLA and PVDF films are piezoelectric materials, but they show dissimilar piezoelectric properties because of their molecular structures and manufacturing processes. The PLLA has helical chain molecules; it exhibits only shear PC after the drawing process[36], so all PLLA films with different CA for four unimodal sensors have no PC with the thickness direction (see Supplementary Note 1. Meanwhile, the PVDF has linear chain molecules; it exhibits three normal PCs (d_{31}, d_{32}, d_{33}) after the drawing and poling process[36], and due to the d_{33}, the PVDF film is sensitive to pressure[12]. Therefore, the PVDF film can not be developed for unimodal sensors, as it is theoretically impossible to eliminate the d_{33} by cutting the PVDF film.

Figure 3c compares the piezoelectric responses of the four unimodal sensors and conventional single-layered PLLA film sensors following the above conditions. Notably, all unimodal sensors exhibit much higher piezoelectric responses than the PLLA sensors under corresponding deformations, but their increased levels are different. Under tensioning and shearing, the $V_{p\text{-}p}$ of the tension and shear sensors almost double compared to the single PLLA film sensors. It is reasonable because the tension and shear sensors consist of two PLLA films, producing coherent piezoelectric signals under the corresponding deformation. For the bend sensor, its $V_{p\text{-}p}$ is twenty times stronger than that of the PLLA45 sensor. Under the same bending curvature, the bend sensor should be subjected to a more significant bending force than the PLLA45 sensor because of the increased thickness. However, the bending force cannot act on the sensor directly because there is no PC along with the thickness direction of the sensor. Instead, the force induces the opposite bending stresses (i.e., compressive stress and tensile stress) and then applies to the sensor to generate the piezoelectricity because of the newly developed piezoelectric coefficients of the length/width directions after cutting. Moreover, the bottom area of the sensor receives the most stress when bent, which is more complex than tensioning/shearing deformation. Thus it produces twenty times more robust signal than the PLLA45 sensor. Similarly, the twist sensor presents a boosted piezoelectric behavior than the PLLA0 sensor; significantly, it shows about seventy times stronger signal than the PLLA0 sensor at a twisted angle of 30°. To further confirm this, we compared the $V_{p\text{-}p}$ of two sensors at twisted angles of 20° and 40°, showing consistent results (Supplementary Fig. 10).

Owing to the capacitive feature of piezoelectric sensors, including the conventional piezoelectric PLLA sensor, they are susceptible to electromagnetic (EM) interference (e.g., 50 Hz EM noise originating from household electricity) and motion artifact in a real-world setting[37]. It is easy to eliminate the 50 Hz EM noise using an appropriate electronic filter system because of the regular frequency. Conversely, most motion artifact caused by the human body has an irregular frequency; it could be challenging to be removed using a particular electronic filter system. Therefore, the piezoelectric sensors themselves should have a proper EM shielding function. Since the outer electrode of each unimodal sensor covers the inner electrode completely and is connected to a metallic shield part of a coaxial cable (see Fig. 1c), it can serve as an EM shielding layer. In contrast to the unshielded PLLA45 sensor, the self-shielded unimodal tension sensor exhibits great noise-screening performance against the 50 Hz EM noise and motion artifact (Fig. 3d and Supplementary Video 2).

Integrated unimodal sensor

We then fabricated the i-US by stacking four unimodal sensors, as shown in Fig. 3e. The i-US was tensioned, bent, twisted, and sheared using the relevant machines. The result proves that the i-US has enough capability to detect and differentiate tensioning, bending, twisting, and shearing deformations, respectively. More importantly, this demonstrates that the four unimodal sensors composing the i-US can work together without evident interference. This is mainly because the individual unimodal sensor is shielded by each outer electrode, not affecting the other. The i-US was also deformed by hand to investigate the practicability. As expected, the i-US can discriminate imposed motions separately, as shown in Supplementary Fig. 11 and Supplementary Video 3. We compared the i-US with other state-of-the-art strain sensors in unimodal mechanical stress sensitivity. As shown in the critical review and analysis in Supplementary Table 1, the strain sensors reported have not demonstrated the function of i-US, which can detect and differentiate the individual forces/stresses and their contributions to the complex motion. The current sensors' structural design and sensing mechanisms have not considered the interactions and coupling effects of different forces/stresses involved in complex motions and deformations. The concept and fabrication techniques of i-US have overcome this critical challenge and achieved the function of detecting and differentiating individual tensioning, bending, shearing, and twisting stresses by eliminating their interactions and coupling effects in the structural design. This function is crucial for motion monitoring and control because the joint force of individual stresses determines the motion trajectory.

Motion detection and differentiation applications

Unlike most piezoelectrics, the piezoelectric PLLA film has no pyroelectricity, which means its signal is not influenced by temperature fluctuation[30,36], presenting the advantage of the i-US in real-life applications. To demonstrate the potential of the unimodal sensors in human motion recognition applications, we fabricated a sleeve with the i-US (i-Sleeve for short) to measure

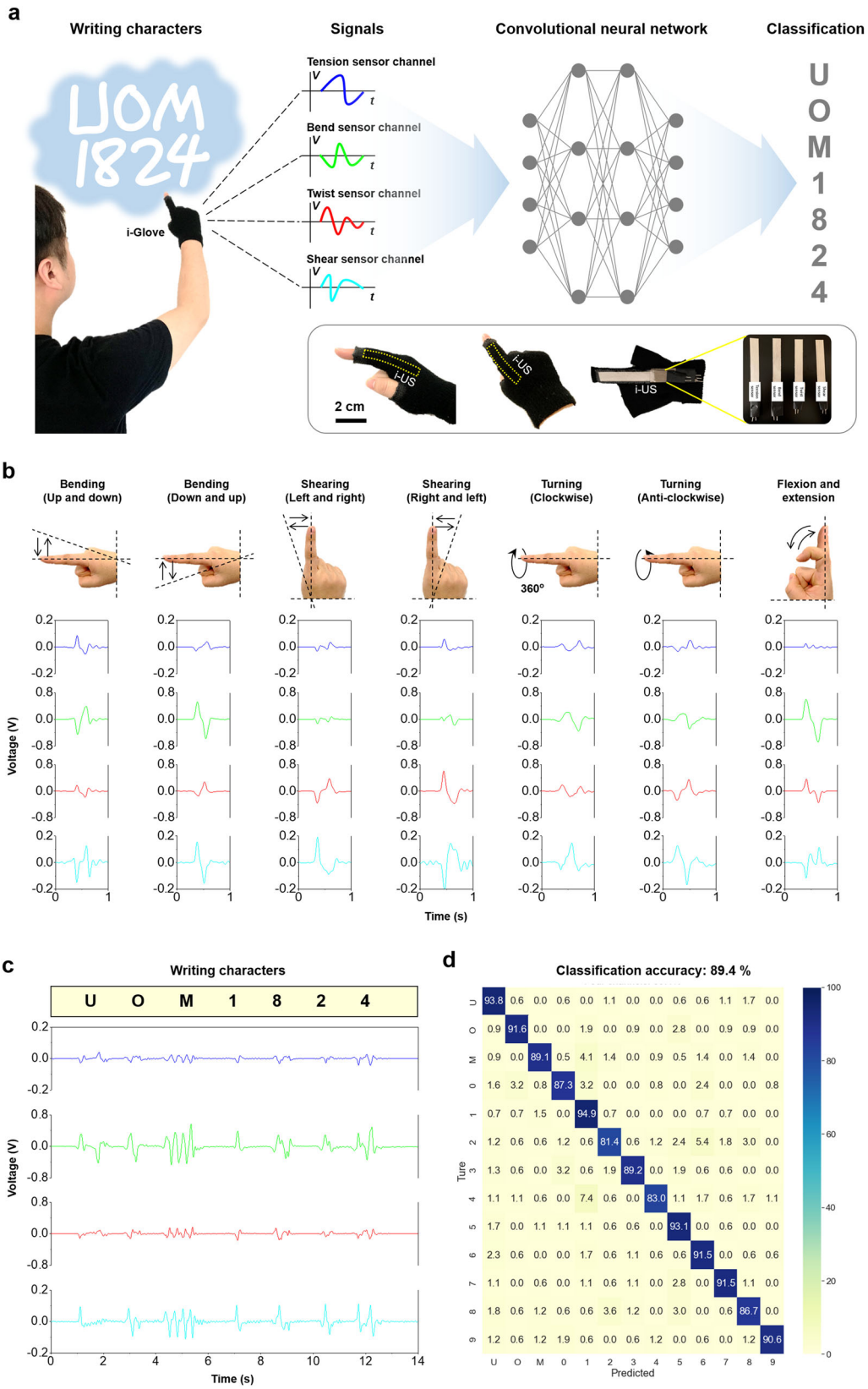

various wrist motions. Since the four unimodal sensors composing the i-US independently respond to their corresponding deformations (tensioning, bending, shearing, and twisting), the i-Sleeve can differentiate complex wrist motions involving multiple degrees of freedom (e.g., extension/flexion, radial/ulnar deviation, pronation/supination) as shown in Supplementary Fig. 12 and Supplementary Video 4. More importantly, a complicated wrist turning action comprising three bending, twisting, and shearing

Fig. 4 Demonstration of an i-US integrated glove (i-Glove) for finger-air-writing application. a Schematic illustration of a finger-air-writing application. A participant wearing the i-Glove writes some characters, e.g., U, O, M, 1, 8, 2, 4, in the free space using his index finger. The four unimodal sensors of the i-US collect the corresponding signal of each character. The acquired signals are input into a pre-trained convolutional neural network (CNN) program after fast fourier transform (FFT). Finally, the program classifies the characters based on the signals. The bottom first two photographs show the i-US positions in the i-Glove at the side and top views. The third photograph shows the inside view of the i-Glove, in which the i-US is inserted into a transparent pocket of the index finger. The last photograph shows four unimodal sensors of the i-US. **b** Index finger motion classification. Top photographs show index finger motions (bending, shearing, turning, and flexion and extension), and the bottom panels show corresponding raw output voltages from four unimodal sensor channels of the i-US. Blue line: tension sensor channel; green line: bend sensor channel; red line: twist sensor channel; cyan line: shear sensor channel. **c** Top panel shows writing characters, and the bottom panel shows corresponding raw output voltages of four unimodal sensor channels of the i-US. All channels are the same as those of **b**. **d** Confusion matrix for the thirteen characters' classification accuracy and its mean accuracy (top) when using four unimodal sensor channels of the i-US.

deformation components is detected simultaneously by the bend, twist, and shear sensor channels. This further implies that the i-US could decouple complex human motions. Supplementary Table 2 summarizes relevant works on wrist motion capture. The i-Sleeve does not require multiple sensors that are distributed to the desired area. It utilizes a single i-US to further identify wrist turning action that is superior to conventional approaches, showing the great efficiency of the i-US.

Furthermore, the i-US was integrated into an index finger of a glove (i-Glove for short) to evaluate its performance in subtle motion recognition (the bottom inset of Fig. 4a), i.e., index finger movements. Due to the limited surface area available on a finger, it is challenging to attach multiple sensors distributed on the desired site. Therefore, most previous studies focused on tracking the fingers' flexion and extension motion (Supplementary Table 3). It is still an open issue to capture index finger movements involving multiple degrees of freedom with strain sensors. The i-US of the i-Glove can discriminate various finger modes, such as bending up and down, shearing left and right, turning clockwise and anti-clockwise, and flexion and extension (Fig. 4b). We then adopted a LeNet-5 based convolutional neural network (CNN) architecture consisting of two convolutional layers to classify the finger motions (Supplementary Fig. 13). Two participants generate the data source of seven finger motions (see Supplementary Methods). The result shows that the mean classification accuracy reaches 90.2% (Supplementary Fig. 14). We also determined the presence or lack of triboelectric effect in finger motion detection. Supplementary Fig. 15 and Supplementary Video 5 show that the triboelectricity in motion detection is undetectable on the scale. This is because the outer electrode of the unimodal sensor is connected to the ground so that it can effectively protect the sensor from triboelectricity, showing the design advantage of the unimodal sensor.

Based on the above findings, we designed a virtual text-entry interface system using the i-Glove in conjunction with the CNN algorithm for a finger-air-writing application, which detects finger movements with the i-US and transforms them into corresponding characters (Fig. 4a, c and Supplementary Video 6). We chose 13 characters (i.e., U, O, M, 0, 1, 2, 3, 4, 5, 6, 7, 8, 9) as target classes. Two participants were invited to create the data source for the finger-air-writing (see Supplementary Methods). As the character's writing style influences the output signal, each character's writing trajectory was strictly defined before collecting data to eliminate the effect (Supplementary Fig. 16). For instance, we instructed the participants to write the letter 'O' in clockwise and the number '0' in anti-clockwise to distinguish them. Supplementary Fig. 17 displays the output data of 13 characters of three trials, which shows good signal reproducibility. The four channels' classification accuracy can reach 89.4% (Fig. 4d). We also examined the classification accuracies of individual sensor channel, two and three-channel combinations. The results show that the testing accuracies increase with the channel numbers; the mean classification accuracy can reach 85.7% when using any three sensor channels (Supplementary Figs. 18–20). Several groups have exploited the vision-based system[7,8] and the inertial sensors[38,39] for air-writing implementation. Unlike these approaches, our finger-air-writing is realized by using the i-US to detect the subtle metacarpophalangeal joint movement of the index finger, demonstrating the performance of the i-US in finger motion monitoring.

In summary, we proposed a concept of film-based flexible unimodal strain sensors for the first time in the world. These unimodal tension, bend, shear, and twist sensors were designed by sticking two uniaxially drawn piezoelectric PLLA films with different CAs, endowing the sensors with unimodal sensing specificity and self-shielding ability. Finally, we demonstrated that these unimodal sensors could detect and differentiate tensioning, bending, twisting, and shearing forces/stresses and identify their impact on the motion trajectory. These unimodal sensors and their combinations can be utilized as force, strain, and deformation sensors with 1, 2, or 3-axial sensitivity, depending on the purpose. We expect the design principle of unimodal piezoelectric sensors proposed here to be applied for other piezoelectrics, making them powerful and intelligent.

METHODS

Piezoelectric response simulations

Parameters used for the piezoelectric response simulations are as follows: a PLLA piezoelectric coefficient (d_{14}) of 10×10^{-12} C·N^−1, a PLLA density of 1250 kg m^−3, a PLLA Young modulus of 4×10^9 Pa, a PLLA Poisson's ratio of 0.36, a PLLA dielectric constant of 3.8. All parameters are estimated values based on the reference[40]. The dimension of the PLLA films (Length × Width × Thickness) is $2 \times 1 \times 0.01$ cm. The applied forces for tensioning, bending, and shearing deformations are 1×10^4 Pa, 1×10^2 Pa, and 1×10^3 Pa, respectively. For twisting deformation, the PLLA film is vertically divided into two parts, and one part applies 1×10^3 Pa and the other part -1×10^3 Pa. The resolution (node numbers: thickness × width × length) of the spatial domain discretization of the PLLA film is $2 \times 21 \times 41$. The bottom of the PLLA film is fixed, and the voltage of one side of the PLLA film is set as zero in finite element simulation. All parameters and applied forces used in these simulations in Fig. 1d are the same as that of the piezoelectric PLLA film simulations of Fig. 1a.

Materials

Ingeo biopolymer 4032D (Mw ≈ 195 000, NatureWorks, USA) with 98% L-isomer and 2% D-isomer was used for uniaxially drawn piezoelectric PLLA film preparation. The PLLA chips are extruded into PLLA film at 225 °C using an extruder after dehumidifying at 120 °C under a vacuum for eight hours. The PLLA film is stretched at different drawing ratios (DR) of 3.3, 3.7, 4.0, and 4.5 by two drawing rollers at about 80 °C, DR is the ratio of linear speeds of the two rollers. Silicon rubber (3140 RTV, Dow Corning, USA) was used for the adhesive, and silver conductive paint (Electrolube SCP03B Conductive Adhesive, WENTWORTH, USA) was used for the electrodes of unimodal sensors.

Output voltage measurement

The output voltages were acquired in the voltage mode of a Piezo Film Lab Amplifier (Measurement Specialties, Inc., USA) in a condition of an input

impedance of 10 MΩ, a band-pass filter range of 0.1–10 Hz, and a gain value of 0 dB. For the shielding performance test (Fig. 3d), the input impedance and the band-pass filter range of the Piezo Film Lab Amplifier increase to 1 GΩ and 0.1–1000 Hz, respectively. For the demonstration of the piezoelectric response of the i-US (Supplementary Fig. 11), a gain value of 20 dB is applied to tension and shear sensor channels. As illustrated in Supplementary Fig. 21, tensioning and shearing deformations were realized using an electromechanical universal testing system (Instron), and bending, and twisting deformations were performed using a bending machine and a twisting machine, respectively.

Characterizations of piezoelectric PLLA films

To determine the crystal orientation and crystallinity of the uniaxially drawn piezoelectric PLLA film, two-dimensional wide-angle x-ray diffraction (2D-WAXD) photograph and the corresponding 1D-WAXD spectrum were obtained in reflection mode using a Rigaku SmartLab 3 K diffractometer with a Cu Kα ($\lambda = 1.54$ Å) radiation source ranging from $2\theta = 4°$ to 40°. Crystallinity percentages of the PLLA films were quantified from the curve deconvolutions of their corresponding 1D-WAXD spectrums. The melting thermograms were measured utilizing a differential scanning calorimeter (DSC Q2000, TA Instruments, USA) at a heating rate of 10 °C/min from 40 to 190 °C at a nitrogen atmosphere. The surface morphology of the PLLA films was analyzed with a field emission scanning electron microscope at an acceleration voltage of 1.5 kV.

Fabrication procedure of two controls

The PLLA chips were dissolved in the chloroform (Alfa Aesar, U.K.) to prepare a PLLA solution (8 wt%). The PLLA solution (60 ml) was poured into a Petri dish (20 cm diameters) and placed the solution in a fume hood at room temperature for 24 h. An unstretched solution cast PLLA film with a thickness of ~130 μm was obtained (Supplementary Fig. 22a). The unstretched PLLA film was then fabricated into two controls with different sizes following the proposed unimodal sensor design concept (Supplementary Fig. 22b).

Signal normalization of unimodal sensors

To compare each unimodal sensor's piezoelectric response at different deformation conditions, its noise signals under unmatched conditions should be considered. As shown in Supplementary Fig. 7, under tensioning deformation, the signals recorded from the bend, twist, and shear sensors are regarded as noises; they are all more significant than the control's signals. Besides, these noises increase with increasing the tensioning deformation level that is directly reflected by the tension sensor. In other words, the noises increase with increasing the signal of the tension sensor. This causes big trouble in comparing each sensor's exact piezoelectric response under different deformations and noise levels. To solve this problem, all $V_{p\text{-}p}$ of the sensors under each deformation level are normalized by dividing the $V_{p\text{-}p}$ of the matched sensor under the same deformation level using Eq. (1)−(4) to place all signals on the same scale (0–1), as summarized in Fig. 3b.

For each tensioning level:

$$V'_{p-p} = \left[\frac{V^{tension}_{p-p}}{V^{tension}_{p-p}}, \frac{V^{bend}_{p-p}}{V^{tension}_{p-p}}, \frac{V^{twist}_{p-p}}{V^{tension}_{p-p}}, \frac{V^{shear}_{p-p}}{V^{tension}_{p-p}}\right] \quad (1)$$

For each bending level:

$$V'_{p-p} = \left[\frac{V^{tension}_{p-p}}{V^{bend}_{p-p}}, \frac{V^{bend}_{p-p}}{V^{bend}_{p-p}}, \frac{V^{twist}_{p-p}}{V^{bend}_{p-p}}, \frac{V^{shear}_{p-p}}{V^{bend}_{p-p}}\right] \quad (2)$$

For each twisting level:

$$V'_{p-p} = \left[\frac{V^{tension}_{p-p}}{V^{twist}_{p-p}}, \frac{V^{bend}_{p-p}}{V^{twist}_{p-p}}, \frac{V^{twist}_{p-p}}{V^{twist}_{p-p}}, \frac{V^{shear}_{p-p}}{V^{twist}_{p-p}}\right] \quad (3)$$

For each shearing level:

$$V'_{p-p} = \left[\frac{V^{tension}_{p-p}}{V^{shear}_{p-p}}, \frac{V^{bend}_{p-p}}{V^{shear}_{p-p}}, \frac{V^{twist}_{p-p}}{V^{shear}_{p-p}}, \frac{V^{shear}_{p-p}}{V^{shear}_{p-p}}\right] \quad (4)$$

where V'_{p-p} is the normalized $V_{p\text{-}p}$, $V^{tension}_{p-p}$ is the $V_{p\text{-}p}$ of the tension sensor under each deformation level, V^{bend}_{p-p} is the $V_{p\text{-}p}$ of the bend sensor, V^{twist}_{p-p} is the $V_{p\text{-}p}$ of the twist sensor, and V^{shear}_{p-p} is the $V_{p\text{-}p}$ of the shear sensor.

Signal collection of the finger motion classification

For the finger motion classification, two sets of i-Glove were prepared and distributed to two participants. Every participant was asked to move the index finger for 100 trials wearing the i-Glove, and all characters were written by fixing the hand while moving the fingers. In each trial, the participants continuously move their fingers following the seven finger modes in Fig. 4b, and the time interval between finger motions is about 2 s. Similarly, for the finger-air-writing, each participant is asked to carry out 100 trials of air-writing wearing the i-Glove. In each test, every participant continuously writes the 13 characters using the index finger following the writing sequence shown in Supplementary Fig. 16. The writing time for each character is about 2 s. The output data of i-US from four channels are recorded at 100 Hz. The collected multi-channel data are then filtered digitally using a sixth-order low-pass Butterworth filter with a 10 Hz cut-off frequency and is segmented using a 1 s sliding window with 0.2 s increment. Since the spectrum of output data from i-US is observed to be less noisy and more distinguishable than the output data in the temporal domain, each segmented data channel is applied for fast Fourier transform (FFT). The transformed data is split into 80% and 20% and used as a training set and test set of CNN, respectively.

DATA AVAILABILITY

The data that support the findings of this study are available from the corresponding authors upon reasonable request.

Received: 7 April 2022; Accepted: 10 July 2022;
Published online: 17 August 2022

REFERENCES

1. Zhu, M. et al. Haptic-feedback smart glove as a creative human-machine interface (HMI) for virtual/augmented reality applications. *Sci. Adv.* **6**, 1–15 (2020).
2. Dong, W. et al. Soft human–machine interfaces: design, sensing and stimulation. *Int. J. Intell. Robot. Appl.* **2**, 313–338 (2018).
3. Song, K. et al. Pneumatic actuator and flexible piezoelectric sensor for soft virtual reality glove system. *Sci. Rep.* **9**, 1–8 (2019).
4. Kim, K. K. et al. A deep-learned skin sensor decoding the epicentral human motions. *Nat. Commun.* **11**, 1–8 (2020).
5. Boutry, C. M. et al. A stretchable and biodegradable strain and pressure sensor for orthopaedic application. *Nat. Electron.* **1**, 314–321 (2018).
6. Sun, T. et al. Decoding of facial strains via conformable piezoelectric interfaces. *Nat. Biomed. Eng.* **4**, 954–972 (2020).
7. Misra, S., Singha, J. & Laskar, R. H. Vision-based hand gesture recognition of alphabets, numbers, arithmetic operators and ASCII characters in order to develop a virtual text-entry interface system. *Neural Comput. Appl.* **29**, 117–135 (2018).
8. Mukherjee, S., Ahmed, S. A., Dogra, D. P., Kar, S. & Roy, P. P. Fingertip detection and tracking for recognition of air-writing in videos. *Expert Syst. Appl.* **136**, 217–229 (2019).
9. Homayounfar, S. Z. & Andrew, T. L. Wearable sensors for monitoring human motion: a review on mechanisms, materials, and challenges. *SLAS Technol.* **25**, 9–24 (2020).
10. Stenlund, T. C. et al. Inter- and intra-tester reliability when measuring seated spinal postures with inertial sensors. *Int. J. Ind. Ergon.* **44**, 732–738 (2014).
11. Dagdeviren, C. et al. Recent progress in flexible and stretchable piezoelectric devices for mechanical energy harvesting, sensing and actuation. *Extrem. Mech. Lett.* **9**, 269–281 (2016).
12. Chorsi, M. T. et al. Piezoelectric biomaterials for sensors and actuators. *Adv. Mater.* **31**, 1–15 (2019).
13. Dai, Y., Hu, H., Wang, M., Xu, J. & Wang, S. Stretchable transistors and functional circuits for human-integrated electronics. *Nat. Electron.* **4**, 17–29 (2021).
14. Wang, W. et al. Strain-insensitive intrinsically stretchable transistors and circuits. *Nat. Electron.* **4**, 143–150 (2021).
15. Chen, L., Fu, J., Wu, Y., Li, H. & Zheng, B. Hand gesture recognition using compact CNN via surface electromyography signals. *Sensors* **20**, 672 (2020).
16. Moin, A. et al. A wearable biosensing system with in-sensor adaptive machine learning for hand gesture recognition. *Nat. Electron.* **4**, 54–63 (2021).

17. Xiang, H. et al. Green flexible electronics based on starch. *npj Flex. Electron.* **6**, 15 (2022).
18. Sengupta, D., Romano, J. & Kottapalli, A. G. P. Electrospun bundled carbon nanofibers for skin-inspired tactile sensing, proprioception and gesture tracking applications. *npj Flex. Electron.* **5**, 1–14 (2021).
19. Collins, D. F., Refshauge, K. M., Todd, G. & Gandevia, S. C. Cutaneous receptors contribute to kinesthesia at the index finger, elbow, and knee. *J. Neurophysiol.* **94**, 1699–1706 (2005).
20. Burke, B. Y. D., Gandevia, S. C. & Macefield, G. Responses to passive movement of receptors in joint, skin and muscle of the human hand. *J. Physiol.* **402**, 347–361 (1988).
21. Tu, Y., Liu, L., Li, M., Chen, P. & Mao, Y. A review of human motion monitoring methods using wearable sensors. *Int. J. Online Eng.* **14**, 168–179 (2018).
22. Huang, B. et al. Wearable stretch sensors for motion measurement of the wrist joint based on dielectric elastomers. *Sensors (Switzerland)* **17**, 2708 (2017).
23. Cha, Y., Seo, J., Kim, J. S. & Park, J. M. Human-computer interface glove using flexible piezoelectric sensors. *Smart Mater. Struct.* **26**, 5 (2017).
24. Araromi, O. A. et al. Ultra-sensitive and resilient compliant strain gauges for soft machines. *Nature* **587**, 219–224 (2020).
25. Souri, H. et al. Wearable and stretchable strain sensors: materials, sensing mechanisms, and applications. *Adv. Intell. Syst.* **2**, 2000039 (2020).
26. Leber, A., Cholst, B., Sandt, J., Vogel, N. & Kolle, M. Stretchable thermoplastic elastomer optical fibers for sensing of extreme deformations. *Adv. Funct. Mater.* **29**, 1–8 (2019).
27. Chander, H. et al. Wearable stretch sensors for human movement monitoring and fall detection in ergonomics. *Int. J. Environ. Res. Public Health* **17**, 1–18 (2020).
28. Jeong, S. M. et al. Development of multi-angle fiber array for accurate measurement of flexion and rotation in human joints. *npj Flex. Electron.* **5**, 1–12 (2021).
29. Fukada, E. Recent developments of polar piezoelectric polymers. *IEEE Trans. Dielectr. Electr. Insul.* **13**, 1110–1119 (2006).
30. Ando, M., Kawamura, H., Kageyama, K. & Tajitsu, Y. Film sensor device fabricated by a piezoelectric poly(L-lactic acid) film. *Jpn J. Appl. Phys.* **51**, 1–4 (2012).
31. Curry, E. J. et al. Biodegradable piezoelectric force sensor. *Proc. Natl Acad. Sci. USA* **115**, 909–914 (2018).
32. Fukada, E. History and recent progress in piezoelectric polymers. *IEEE Trans. Ultrason. Ferroelectr. Freq. Control* **47**, 1277–1290 (2000).
33. Ru, J. F. et al. Dominant β-form of poly(l -lactic acid) obtained directly from melt under shear and pressure fields. *Macromolecules* **49**, 3826–3837 (2016).
34. Yin, H. M. et al. Effects of extrusion draw ratio on the morphology, structure and mechanical properties of poly(L-lactic acid) fabricated using solid state ram extrusion. *RSC Adv.* **5**, 69016–69023 (2015).
35. Tao, K. et al. Bioinspired stable and photoluminescent assemblies for power generation. *Adv. Mater.* **31**, 1–7 (2019).
36. Smith, M. & Kar-Narayan, S. Piezoelectric polymers: theory, challenges and opportunities. *Int. Mater. Rev.* **0**, 1–24 (2021).
37. Atalay, A. et al. Batch fabrication of customizable silicone-textile composite capacitive strain sensors for human motion tracking. *Adv. Mater. Technol.* **2**, 1–8 (2017).
38. Amma, C., Georgi, M. & Schultz, T. Airwriting: Hands-free mobile text input by spotting and continuous recognition of 3d-space handwriting with inertial sensors. *Proc. - Int. Symp. Wearable Comput. ISWC* 52–59 https://doi.org/10.1109/ISWC.2012.21 (2012).
39. Chen, M., AlRegib, G. & Juang, B. H. Air-writing recognition - Part I: modeling and recognition of characters, words, and connecting motions. *IEEE Trans. Hum.-Mach. Syst.* **46**, 403–413 (2016).
40. Smith, M., Calahorra, Y., Jing, Q. & Kar-Narayan, S. Direct observation of shear piezoelectricity in poly-l-lactic acid nanowires. *APL Mater.* **5** (2017).
41. Muller, J., González-Martínez, C. & Chiralt, A. Combination Of Poly(lactic) acid and starch for biodegradable food packaging. *Mater. (Basel)* **10**, 1–22 (2017).

ACKNOWLEDGEMENTS

This work was financially supported by the EU Horizon 2020 through project ETEXWELD-H2020-MSCA-RISE-2014 (Grant No. 644268), the University of Manchester through the UMRI project-Graphene-Smart Textiles E-Healthcare Network (Grant No. AA14512) and the Engineering and Physical Sciences Research Council (EPSRC) of UK (Grant EP/V057782/1).

AUTHOR CONTRIBUTIONS

The work was conceived and designed by L.J., Y.L., and K.J.K. L.J. performed the mathematical model and the piezoelectric response simulations and discussed them with Y.L. and K.J.K. H.K. and K.J.K. prepared the uniaxially drawn piezoelectric PLLA film. L.J. and L.X. supervised sensor fabrication. Z.L. and C.D. ran the piezoelectric response test. Y.Z. assisted with the shielding performance test. H.Z. and P.Y. performed the XRD experiment. J.L. prepared the unstretched solution cast PLLA film. L.J. and Q.S. fabricated the i-Sleeve and i-Glove. Z.L. and S.Q.X. performed the CNN. L.J. drafted the manuscript, Y.L., K.J.K., S.Q.X., Z.L., and B.R. revised the manuscript, and all authors discussed the results.

COMPETING INTERESTS

The authors declare no competing interests.

ADDITIONAL INFORMATION

Supplementary information The online version contains supplementary material available at https://doi.org/10.1038/s41528-022-00205-4.

Correspondence and requests for materials should be addressed to Qingwen Song, Sheng Quan Xie, Kap Jin Kim or Yi Li.